How much primordial tensor mode is allowed?

Moumita Aich,[1,*] Yin-Zhe Ma,[2,3,†] Wei-Ming Dai,[2,3,‡] and Jun-Qing Xia[4,§]

[1]*School of Mathematics, Statistics and Computer Science, University of KwaZulu-Natal, Durban 4000, South Africa*

[2]*School of Chemistry and Physics, University of KwaZulu-Natal, Durban 4000, South Africa*

[3]*NAOC-UKZN Computational Astrophysics Centre (NUCAC), University of KwaZulu-Natal, Durban 4000, South Africa*

[4]*Department of Astronomy, Beijing Normal University, Beijing 100875, China*

(Received 2 December 2019; accepted 9 March 2020; published 30 March 2020)

The presence of a significant amount of gravitational radiation in the early Universe affects the total energy density and hence the expansion rate in the early epoch. In this work, we develop a physical model to connect the number of relativistic degrees of freedom $N_{\rm eff}$ with the amplitude and shape of the primordial tensor power spectrum, and use the cosmic microwave background temperature and polarization data from *Planck* and the BICEP2/KECK Array and the primordial deuterium measurements from damped Lyman-α systems to constrain this model. We find that with the extra relation $\Delta N_{\rm eff}(r, n_{\rm t})$, the tensor-to-scalar ratio r is constrained to be $r < 0.07$ (3σ C.L.) and the tilt of the tensor power spectrum is $n_{\rm t} = -0.01 \pm 0.31$ (1σ C.L.) for $Planck + {\rm BICEP2} + {\rm KECK} + [{\rm D/H}]$ data. This achieves a much tighter constraint on the tensor spectrum and provides a stringent test for cosmic inflation models. In addition, the current constraint on $N_{\rm eff} = 3.122 \pm 0.171$ excludes the possibility of a fourth neutrino species at more than 5σ C.L.

DOI: 10.1103/PhysRevD.101.063536

I. INTRODUCTION

The detection of the large-angular-scale B-mode polarization of the cosmic microwave background (CMB) is one of the current challenges in modern observational cosmology. The B-mode polarization signal arises only from tensor perturbations in the early Universe and is a direct signature of inflationary gravitational waves (GWs). The tensor perturbation power spectrum can be parametrized as

$$P_{\rm t}(k) = A_{\rm t}(k_0)\left(\frac{k}{k_0}\right)^{n_{\rm t}+(\alpha_{\rm t}/2)\ln(k/k_0)} = rA_{\rm s}(k_0)\left(\frac{k}{k_0}\right)^{n_{\rm t}+(\alpha_{\rm t}/2)\ln(k/k_0)}, \quad (1)$$

where $A_{\rm s}(k_0)$ is the primordial scalar fluctuation amplitude, $r(k_0) = A_{\rm t}(k_0)/A_{\rm s}(k_0)$ is the tensor-to-scalar ratio at a pivot scale k_0, $n_{\rm t}$ is the spectral index of the tensor power spectrum, and $\alpha_{\rm t}$ is the running of the spectral index. For the single-field slow-roll inflation model the generic consistency relation $r = -8n_{\rm t}$ is satisfied. A power spectrum with a small negative tilt (red tilt, $n_{\rm t} < 0$) is thus a characteristic prediction for single-field slow-roll inflation models [1]. Testing this prediction by using CMB and big bang nucleosynthesis (BBN) data is an essential task to pin down the uncertainty of inflationary models.

The consistency relation is, however, not satisfied for multifield inflation and models which deviate from slow roll. Alternative cosmological models, such as string gas cosmology [2], superinflation models [3], and many others not yet ruled out by observations, predict a blue tilt ($n_{\rm t} > 0$) of the GW spectrum, i.e., more power at small scales. Therefore, observational constraints on the tilt of the tensor spectrum would be worth investigating since it has the distinguishing power in model space [2,4–7]. It is thus appropriate to use a phenomenological approach by relaxing the consistency relation. Even though a direct detection of the inflationary GW background is yet to be achieved, the current CMB measurement from *Planck*, the Background Imaging of Cosmic Extragalactic Polarization (BICEP2) telescope, and KECK Array data are already able to constrain it to a certain level [8–12]. Apart from the CMB, other observational techniques also provide constraints on the stochastic GWs at different frequencies, through BBN [13,14], pulsar timing [15–18], and more directly through the Laser Interferometer Gravitational-wave Observatory (LIGO) and Virgo interferometer GW detectors [19].

A blue-tilted tensor power spectrum would lead to additional small-scale relativistic degrees of freedom [4,7,17,20], changing the energy density of the Universe,

*aich@ukzn.ac.za
†ma@ukzn.ac.za
‡daiw@ukzn.ac.za
§xiajq@bnu.edu.cn

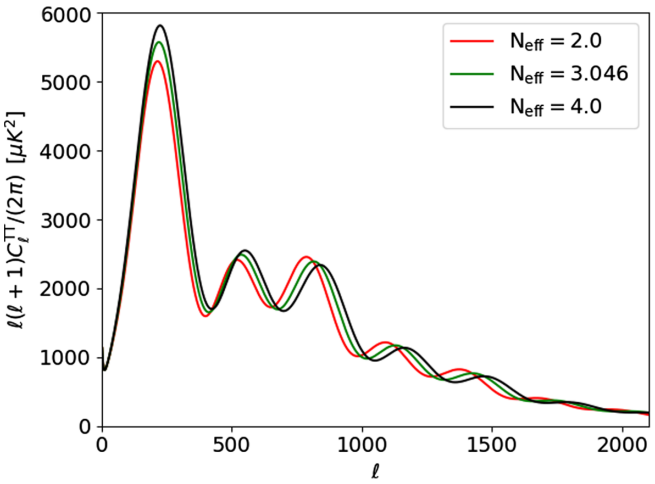

FIG. 1. The effect of $N_{\rm eff}$ (number of relativistic species) on the CMB temperature power spectrum. We fix all other cosmological parameters as $\Omega_{\rm b}h^2 = 0.0224$, $\Omega_{\rm c}h^2 = 0.1201$, $\Omega_\nu h^2 = 0.6451 \times 10^{-3}$, $\Omega_k = 0$, $H_0 = 67.32\ {\rm km\,s^{-1}\,Mpc^{-1}}$, and $A_{\rm s} = 2.1 \times 10^{-9}$.

which in turn would affect the expansion rate during that era. Relativistic neutrinos also contribute to the energy density of the Universe, and the modification of the neutrino energy density can be parametrized by the effective number of neutrino species $N_{\rm eff}$. The effect of the tensor blue tilt is thus degenerate with $N_{\rm eff}$. The Standard Model of particle physics predicts $N_\nu = 3.046$, so any value of $N_{\rm eff}$ other than N_ν can be attributed to either an additional species of neutrino or the gravitational-wave background. This radiation density has major ramifications for various early Universe physical processes, leaving detectable imprints on the CMB at the epoch of last scattering. Figure 1 shows the effect of the parameter $N_{\rm eff}$ on the CMB temperature anisotropies. The major physical effects are as follows.

(1) Delaying matter-radiation equality [21–25]: As $N_{\rm eff}$ increases, the fractional density of radiation increases, and therefore matter-radiation equality occurs later. The magnitude of the early integrated Sachs-Wolfe (ISW) effect changes if the matter-radiation equality epoch changes. The earlier the matter-radiation equality epoch is, the greater the ISW effect that CMB photons receive [24,25]. The effect can be measured through the ratio between the heights of the third and first acoustic peaks of $C_\ell^{\rm TT}$, leading to the extraction of $z_{\rm eq}$ directly via the CMB power spectrum [25]. By using the relation of the present-day neutrino temperature and CMB temperature as $T_\nu = (4/11)^{1/3}T_\gamma$, one can derive the equality epoch as [24,25]

$$1 + z_{\rm eq} = \frac{\Omega_{\rm m}h^2}{\Omega_\gamma h^2}\frac{1}{1 + 0.2271N_{\rm eff}}, \qquad (2)$$

where the radiation energy density $\Omega_\gamma h^2 = 2.47 \times 10^{-5}$, and the present-day CMB temperature is $T_\gamma = 2.725$ K. As one can see from Eq. (2), $\Omega_{\rm m}h^2$ and $N_{\rm eff}$ are linearly correlated with each other, and the width of the degeneracy dependent on the uncertainty of $z_{\rm eq}$. The anisotropic stress of the relativistic degrees of freedom can break the degeneracy by imprinting distinct features on the CMB sky, independent of $\Omega_{\rm m}h^2$.

(2) Adding anisotropic stress: Acoustic stress from relativistic particles adds to the gravitational potential as an additional source of energy via Einstein's equations [25]. In comparison, those relativistic particles that do not stream freely, but rather interact with matter frequently, do not have significant anisotropic stress because they isotropize themselves via interacting with matter. Therefore, the anisotropic stress of photons before the decoupling time is very small. However, neutrinos and gravitons decouple from the hot plasma very early on, so the anisotropic stress is significant at the decoupling epoch. This effect is uncorrelated with $\Omega_{\rm m}h^2$, and therefore it can break the degeneracy.

(3) Changing the sound horizon: In the standard cosmological model, free-streaming neutrinos travel supersonically through the photon-baryon plasma after their decoupling ($T \sim 1$ MeV), so they gravitationally pull the wave fronts of the plasma oscillation slightly ahead in time compared to when neutrinos are absent [26–30]. Therefore, the free-streaming neutrinos change the phase of the CMB acoustic oscillations by shifting the power spectra towards larger angular scales (smaller ℓ), while also suppressing the damping tail. Similar to neutrinos, any relativistic degrees of freedom also have a similar effect of altering the scale of the sound horizon, thus causing the distinctive shift in the CMB power spectra [26–30].

In Fig. 1, we plot the effect of $N_{\rm eff}$ on the CMB temperature power spectrum, with all other cosmological parameters fixed. One can clearly see the distinct change of the power spectrum due to the combination of all three of the above-mentioned effects. To see each effect, one needs to fix the sound horizon, or fix $z_{\rm eq}$ and vary $N_{\rm eff}$. We refer the interested reader to Fig. 1 in Ref. [29], Fig. 1 in Ref. [30], Fig. 2 in Ref. [27], and Fig. 1 in Ref. [26].

High-precision CMB observations—such as those from the space-based *Wilkinson Microwave Anisotropy Probe* (WMAP) [31] and *Planck* satellite [10,32], the ground-based Atacama Cosmology Telescope [33,34], the South Pole Telescope [35,36], the BICEP2-KECK Array [11,12], and the balloon-based SPIDER [37–39]—have the potential to provide rigorous constraints on the neutrino background. Therefore, these experiments should also be able to place strong constraints on extra relativistic degrees of

freedom caused by a blue-tilted tensor power spectrum. In this paper we first explore ways to constrain the effective relativistic species using current CMB data from *Planck* and the BICEP2/KECK Array; we call this the "CMB with $\Delta N_{\rm eff}$ relation" case.

Beside the effect on the CMB, the relative abundances of primordial light elements such as hydrogen (H), deuterium (D), helium-3 (^{3}He), helium-4 (^{4}He), and small amounts of lithium-7 (^{7}Li) created during BBN are also strongly affected by the GW background. Significant gravitational radiation during primordial nucleosynthesis affects the total energy density of the Universe, which alters the expansion rate of the Universe. Thus, if the GW background is modified the relative abundances of the light elements would vary from the predictions of standard BBN. This is an indirect constraint on the energy density of the GW background [4].

Constraints on $N_{\rm eff}$ from CMB measurements are mostly derived from measurements of the damping tail [8,40,41]. An increase in the radiation density of the early Universe reduces the mean free path of fluctuations in the photon baryon fluid and increases the damping of small-scale fluctuations. Changes to the helium and deuterium fraction ($Y_{\rm p}$ and D/H) induce a variation in the free electron fraction, which in turn alters the mean free path of the photons and affects the damping tail [42]. We use the D/H measurements from Refs. [43,44], complemented by the *Planck* and BICEP2/KECK likelihoods to study the constraints on $N_{\rm eff}$ and consequently the effect on the $r - n_{\rm t}$ joint distribution: we call this the "CMB + D/H with $\Delta N_{\rm eff}$ relation" case.

The paper is organized as follows. In Sec. II we discuss the relation between the primordial GW energy density and the effective degrees of freedom of relativistic species. Then, we discuss how does this $\Delta N_{\rm eff}$ impacts helium production. In Sec. III we introduce the data sets we use for our analysis, i.e., CMB data from the *Planck* satellite and the BICEP2/KECK Array 2018 release. We also use deuterium abundance data from damped Lyman-α systems (DLAs) which serve as an independent measurement of $N_{\rm eff}$. In Sec. IV we present the results of our Markov chain Monte Carlo runs and their implication. Our conclusion and future goals are presented in Sec. V. Throughout the paper we adopt a spatially flat ΛCDM cosmology model with adiabatic initial conditions.

II. RELATIVISTIC DEGREES OF FREEDOM

Stochastic GW background searches venture to measure the fractional energy density of GWs as a function of frequency. We define the logarithmic GW contribution to the critical density as [14,45]

$$\Omega_{\rm GW}(k) \equiv \frac{1}{\rho_{\rm c}} \frac{{\rm d}\rho_{\rm GW}}{{\rm d}\ln k}, \tag{3}$$

where $\rho_{\rm GW}$ is the frequency (wave number k)-dependent effective energy density, and $\rho_{\rm c} = 3c^2H_0^2/8\pi{\rm G}$ is the critical density of the Universe at present, where $H_0 \equiv 100h$ km s^{-1} Mpc^{-1} is the current Hubble parameter. The GW energy density can be related to h_k, which is the Fourier transform of the metric perturbation, as

$$\Omega_{\rm GW}h^2 = \frac{c^2k^2h^2}{6H_0^2}\langle|h_k^2|\rangle \equiv A_{\rm GW}P_{\rm t}(k), \tag{4}$$

where $A_{\rm GW} = 2.74 \times 10^{-6} g_{100}^{-1/3}$, where $g_{100} \equiv g_*(T_{\rm k})/100$ is the degree of freedom at the time when GWs are stretched outside of the Hubble radius. If we only count Standard Model particles, then $g_*(T_k) = 106.75$, and so $g_{100} = 1.06$ [46].

In the early Universe before BBN, gravitons behave like relativistic particles whose density $\sim a^{-4}$. Thus, if there were too many gravitons before BBN, it would substantially enhance the total energy density of the Universe, thus making the Universe expand too fast. First, we need to calculate the GW density back to the time of BBN.

A. Energy densities

The energy densities for neutrinos, gravitons, and photons are given as

$$\begin{aligned}
\rho_\nu &= \frac{7}{8}\frac{\pi^2}{15} N_\nu T_\nu^4, \\
\rho_{\rm G} &= \frac{7}{8}\frac{\pi^2}{15} \Delta N_{\rm eff} T_\nu^4, \\
\rho_\gamma &= \frac{\pi^2}{15} T_\gamma^4,
\end{aligned} \tag{5}$$

in which we assume that the graviton spin is 2. The neutrino temperature is related to the CMB temperature as $T_\nu = (4/11)^{1/3}T_\gamma$, where we take $T_\gamma = 2.726$ K. At the time of BBN,

$$\rho_{\rm c}(t_{\rm n}) = \rho_\gamma(t_{\rm n}) + \rho_\nu(t_{\rm n}), \tag{6}$$

$$\frac{\rho_{\rm c}(t_{\rm n})}{\rho_\gamma(t_{\rm n})} = \frac{N_\nu \frac{7}{8}(\frac{4}{11})^{4/3} + 1}{1} \simeq 1.692. \tag{7}$$

We integrate Eq. (4) over all possible scales and use Eq. (5) to calculate the increment of the effective number of relativistic species back to the time of BBN,

$$\begin{aligned}
\Delta N_{\rm eff} &= \frac{8}{7}\left(\frac{11}{4}\right)^{4/3} \frac{A_{\rm GW}}{h^2} \frac{\rho_{\rm c}(t_{\rm n})}{\rho_\gamma(t_{\rm n})} \int_{\ln k_{\rm min}}^{\ln k_{\rm max}} {\rm d}\ln k P_{\rm t}(k) \\
&= 1.781 \times 10^5 A_{\rm GW} \int_{\ln k_{\rm min}}^{\ln k_{\rm max}} {\rm d}\ln k P_{\rm t}(k).
\end{aligned} \tag{8}$$

B. The integral

To evaluate the integral in Eq. (8), we need to figure out the upper and lower limits of the wave number k. We set $k_{\rm min}$ as the particle horizon of the Universe at the time of BBN, so $k_{\rm min} \simeq k_{H_{\rm BBN}}$. $k_{\rm max}$ corresponds to the minimal scale of the perturbation, which entered the Hubble radius right after inflation, so we that assume $k_{\rm max} = e^{60} k_{H_0}$, where

$$k_{H_0} = \frac{2\pi}{(\frac{c}{H_0})} = \frac{2\pi H_0}{c} = 0.0015\ \text{Mpc}^{-1}. \tag{9}$$

If we assume that $H_0 = 70\ \text{kms}^{-1}\ \text{Mpc}^{-1}$, then

$$k_{\rm min} = \frac{2\pi}{(\frac{c}{H_{\rm BBN} a_{\rm BBN}})} = \frac{2\pi H_{\rm BBN} a_{\rm BBN}}{c}, \tag{10}$$

$$\begin{aligned} H^2_{\rm BBN} &= \frac{8\pi G}{3}(\rho_\gamma + \rho_\nu) \\ &= \frac{8\pi G}{3}\rho_\gamma (1 + 0.2271 N_{\rm eff}) \\ &\simeq \frac{8\pi G}{3} \times 1.69 \times \rho_\gamma, \end{aligned} \tag{11}$$

where for the second line we used Eq. (5). Since

$$\frac{\rho_\gamma}{\rho_{\rm cr}} = \frac{2.47 \times 10^{-5}}{h^2 a^4}, \tag{12}$$

we have

$$H_{\rm BBN} = H_0 \times \left[\frac{6.46 \times 10^{-3}}{h a^2}\right]. \tag{13}$$

Therefore, we have

$$\begin{aligned} k_{\rm min} &= 2\pi \left(\frac{H_{\rm BBN} a_{\rm BBNc}}{c}\right) \\ &= \left(2\pi \frac{H_0}{c}\right)\left(\frac{6.46 \times 10^{-3}}{h a_{\rm BBN}}\right), \end{aligned} \tag{14}$$

where $a_{\rm BBN} = T_0/T_{\rm BBN} \simeq 2.275\ \text{K}/1\ \text{MeV} = 1.96 \times 10^{-10}$ and $h = 0.7$. Thus,

$$k_{\rm min} = 4.7 \times 10^7 \left(2\pi \frac{H_0}{c}\right) = 6.9 \times 10^4\ \text{Mpc}^{-1}. \tag{15}$$

Now let us focus on calculating the integral

$$I_1(n_{\rm t}, \alpha_{\rm t}) = \int \text{d} \ln k \left(\frac{k}{k_0}\right)^{n_{\rm t} + (1/2)\alpha_{\rm t} \ln(k/k_0)}, \tag{16}$$

which is found to be

$$\begin{aligned} I_1(n_{\rm t}, \alpha_{\rm t}) = e^{-(n_{\rm t}/\alpha_{\rm t})^2/2} &\left(\frac{\pi}{-2\alpha_{\rm t}}\right)^{1/2} \\ &\times \left[\text{Erf}\left(\sqrt{-\frac{\alpha_{\rm t}}{2}}\left(\ln\left(\frac{k_{\rm max}}{k_0}\right) + \frac{n_{\rm t}}{\alpha_{\rm t}}\right)\right)\right. \\ &\left. - \text{Erf}\left(\sqrt{-\frac{\alpha_{\rm t}}{2}}\left(\ln\left(\frac{k_{\rm min}}{k_0}\right) + \frac{n_{\rm t}}{\alpha_{\rm t}}\right)\right)\right], \end{aligned} \tag{17}$$

where "Erf" represents for error function.

We consider $\alpha_{\rm t} = 0$, given that the current CMB data does not point to any strong evidence of the running of the tensor tilt. Combining the above equations, we find

$$\Delta N_{\rm eff}(r, n_{\rm t}) = 1.781 \times 10^5 A_{\rm GW} A_{\rm s}(k_0) r I_1(n_{\rm t}), \tag{18}$$

where

$$\begin{aligned} I_1(n_{\rm t}) &= \frac{1}{n_{\rm t}}\left[\left(\frac{k_{\rm max}}{k_0}\right)^{n_{\rm t}} - \left(\frac{k_{\rm min}}{k_0}\right)^{n_{\rm t}}\right], \quad \text{if } n_{\rm t} \neq 0, \\ &= \ln\left(\frac{k_{\rm max}}{k_{\rm min}}\right), \quad \text{if } n_{\rm t} = 0. \end{aligned} \tag{19}$$

Here

$$\begin{aligned} k_{\rm max} &= \text{e}^{60} k_{H_0} \simeq 1.67 \times 10^{23}\ \text{Mpc}^{-1}, \\ k_{\rm min} &= 6.9 \times 10^4\ \text{Mpc}^{-1}, \end{aligned} \tag{20}$$

and we take the pivot scale as $k_0 = 0.01\ \text{Mpc}^{-1}$ to be consistent with *Planck* [10]. Figure 2 shows $\Delta N_{\rm eff}$ as a function of $n_{\rm t}$ for different values of r and $\alpha_{\rm t}$. We plot the current 95% confidence level (C.L.) upper limit of r as $r < 0.1$ from the constraints from *Planck* TT + TE + EE + lowE + lensing [10], and the cosmic variance limit of r as $r = 10^{-3}$ [47]. The horizontal black dashed line shows $\Delta N_{\rm eff} < 0.17$ as the 68% C.L. upper limit [10]. One can see that, even if the value of r is small, the blue-tilted $n_{\rm t}$ can

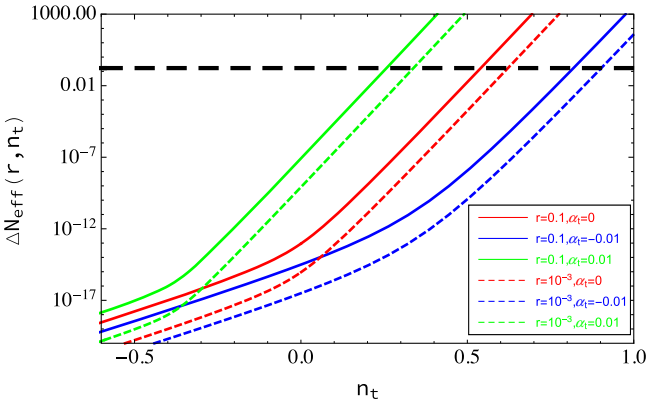

FIG. 2. The increment of the effective number of relativistic species given the value of $n_{\rm t}$. The three curves show the assumed value of $\alpha_{\rm t}$. The horizontal dashed line shows the current 1σ limit of $\Delta N_{\rm eff}$ [10].

lead to a large increment of $\Delta N_{\rm eff}$, resulting in an observable effect on the CMB and light element abundance.

C. Helium abundance

Given a set of cosmological parameters, the primordial abundance of light elements is fully computable from the Standard Model of particle physics [48]. The precise determination of the cosmological parameters from the *Planck* satellite led to accurate predictions of the light element abundances, such as ^{4}He from low-metallicity H$_{\rm II}$ regions in low-redshift star-forming galaxies [49,50], the primordial abundance of deuterium (D/H) using quasar absorption lines like the DLAs [43,44,51], and the ^{7}Li/H ratio in metal-poor stars in the Milky Way halo [52]. The standard BBN populations of relativistic particles—including photons, electrons, positrons, and three species of neutrinos—mix as a hot plasma with the same temperature. At a given temperature, the resulting cosmic expansion rate is 2.3 times that for photons alone. The weak freeze-out starts at this time, establishing the neutron-to-proton ratio which eventually determines the helium abundance $Y_{\rm p}$. Additional relativistic degrees of freedom can enhance the expansion rate by a factor of 8%,[1] which forces the neutrino freeze-out to occur at a higher temperature. This, in turn, implies more neutrons, triggering more ^{4}He.

By modifying the publicly available PArthENoPE 2.0 code,[2] we implement the $\Delta N_{\rm eff}(r, n_{\rm t})$ relation into the code and output the helium abundance as a function of $n_{\rm t}$ by fixing the r value. In Fig. 3 we plot the helium abundance as a function of $n_{\rm t}$ for the cases of $r = 10^{-3}$ and $r = 0.1$. The $\Delta N_{\rm eff}$ values are marked on the upper horizontal axis. One can see that as $n_{\rm t}$ goes from negative values to slightly positive values, the $\Delta N_{\rm eff}$ increases dramatically, leading to a higher temperature of neutrino freeze-out. This will lead to more helium production. However, there is a downward branch of $Y_{\rm p}$ when $n_{\rm t} \gtrsim 0.5$. This is because, if $n_{\rm t}$ becomes very positive, the $N_{\rm eff}$ value becomes exponentially large, and thus the Hubble expansion during the early Universe becomes too fast to allow nucleons to interact and form helium. The Universe would then cool down too soon for nuclei to form helium. Therefore, for $n_{\rm t} \gtrsim 0.5$, i.e., $\Delta N_{\rm eff} \gtrsim 10^3$, the helium production becomes much lower than in the Standard Model.

Current measurements from observations of the helium and hydrogen emission lines from metal-poor extragalactic H$_{\rm II}$ regions, combined with the estimated metallicity, give the primordial helium abundance as [49]

$$Y_{\rm p} = 0.2449 \pm 0.0040, \tag{21}$$

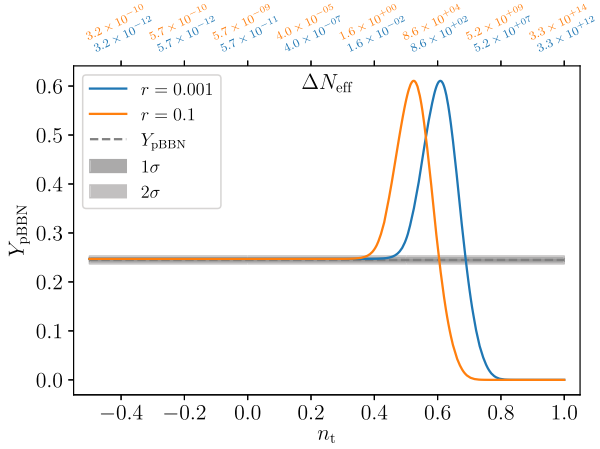

FIG. 3. The abundance of helium ($Y_{\rm p}$) as a function of $n_{\rm t}$. The blue and orange lines are for $r = 10^{-3}$ and $r = 0.1$, respectively. The horizontal grey band is the current measurement of $Y_{\rm p}$ [Eq. (21)] from Ref. [49].

which is shown as the horizontal grey band in Fig. 3. Large systematic uncertainties and degeneracies among the input parameters needed to model emission line fluxes limit the measurements. Along with this large-error-bar predicament, this also results in a 2σ deviation from the standard ΛCDM prediction [49,50,53]. More recently, $Y_{\rm p}$ was determined from measurements of the absorption lines of intergalactic gas clouds against the light from a background quasar [44], though the measurement error is still quite large. Due to these reasons, in the next section we will only use measurements of deuterium abundance to constrain the $\Delta N_{\rm eff}$ relation.

III. DATA

A. Deuterium abundance

The deuterium abundance is also closely related to the number of relativistic species that existed during BBN. The abundance of deuterium is determined by the $d + d$ and $d + p$ reactions towards the end of BBN when the photon temperature drops below the rest mass of the electron. Therefore, there are essentially no electrons or positrons at this time, and their annihilation heats the photons. The expansion rate at this time is ∼1.7 times that for just photons, and an additional $N_{\rm eff}$ would increase the rate of cosmic expansion. This would lead to less time for deuterium to burn, and thus a higher D/H [42].

The deuterium abundance is now more precisely measured than $Y_{\rm p}$ by a significant factor through the analysis of the most metal-poor DLA systems, which also display the Lyman series absorption lines of neutral deuterium [43,44,51]. The primordial abundance of deuterium, on the other hand, has a monotonic response to $\Omega_{\rm b,0}h^2$, and accurate measurements of the primordial D/H ratio complemented by measurements of $\Omega_{\rm b,0}h^2$ from the CMB can

[1]The value for the enhanced expansion rate due to an additional neutrino species quoted in Sec. 2. B. in Ref. [42] is 40.3%, which we believe to be an error.

[2]http://parthenope.na.infn.it.

provide a much more sensitive constraint on the allowed values of $N_{\rm eff}$ [42,51].

We use the D/H measurements from Ref. [44] complemented with *Planck* and BICEP2/KECK likelihoods to study the constraints on $N_{\rm eff}$ and consequently the effect on the $r - n_{\rm t}$ joint distribution. The most recent measurement of the cosmic deuterium abundance [44] is derived from six damped Lyman-alpha systems, and is given as

$$10^5({\rm D/H})_{\rm P} = 2.527 \pm 0.030. \tag{22}$$

We use the above measurements from Ref. [44] as a primordial element abundance data set and likelihood in CosmoMC. We also use the updated theory table with reduced errors from Ref. [54] and the publicly available PArthENoPE 2.0 code [55] to compute the abundances of light elements produced during BBN as a function of baryon density and the number of radiation degrees of freedom.

The relation between the deuterium abundance and $\Delta N_{\rm eff}$ is [Eqs. (8)–(10) in Ref. [43]]

$$\eta_{\rm D} = 6\left[\frac{10^5({\rm D/H})_{\rm P}}{2.47}\right]^{-1/1.68} \tag{23}$$

and

$$\Delta N_{\rm eff} = \frac{43}{7}\left[\left(1 + \frac{\eta_{10} - \eta_{\rm D}}{1.08(1.1\eta_{10} - 1)}\right)^2 - 1\right], \tag{24}$$

where

$$\eta_{10} = (273.78 \pm 0.18) \times \Omega_{\rm b}h^2. \tag{25}$$

In Fig. 4 we plot the relation between $\Delta N_{\rm eff}$ and the deuterium abundance $y \equiv 10^5({\rm D/H})_{\rm p}$ by using Eqs. (23)–(25). We allow $\Omega_{\rm b}h^2$ ($\Omega_{\rm b}h^2 = 0.02236 \pm 0.00015$ according to *Planck* TT + TE + EE [10]) and the front factor in Eq. (25) to vary within the 1σ C.L., shown by the black band. One can see that a larger $\Delta N_{\rm eff}$ leads to a larger deuterium prediction. The reason is as follows. The deuterium abundance is determined by the $d(d,n)^3{\rm He}$ and $d(p,\gamma)^3{\rm He}$ processes that burn the deuterium at the end of BBN. At this time, the photon temperature is around $T \sim 0.02$ MeV, which is well below the electron rest mass. Therefore, electron-positron annihilation occurs which increases the photon temperature, leading to the gap between the neutrino and photon temperatures $T_\nu = (4/11)^{1/3}T_\gamma$. The expansion rate at this time in standard BBN is 1.3 times that of photons alone, and the presence of an additional neutrino species at the same temperature as the others increases the rate by 7%. A faster expansion rate means there is less time to burn deuterium, leading to a higher value for D/H.[3] The horizontal red lines are the $\pm 1\sigma$ measurements of Eq. (22). From Fig. 4 one can see that $\Delta N_{\rm eff} \sim 0.3$ is preferred by comparing theory and measurements. The D/H data set described above is incorporated into CosmoMC through a supplementary likelihood and data set with mean and error given as in Eq. (22) and a theory table with D/H abundances as a function of $\Omega_{\rm b}h^2$ as given in the PArthENoPE_880.2_marcucci.dat data set in CosmoMC. We use this D/H data set along with CMB data sets from *Planck* and BICEP2/KECK.

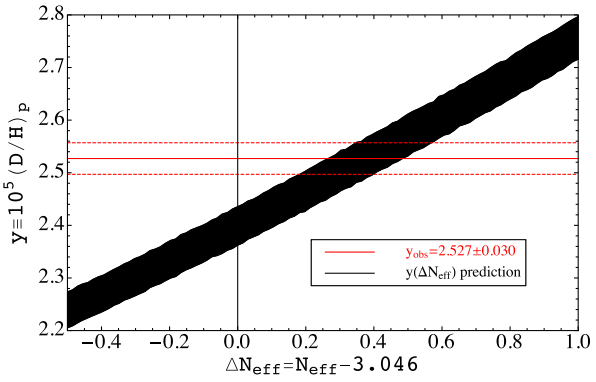

FIG. 4. The relationship between the deuterium prediction and $\Delta N_{\rm eff}$.

B. CMB data from *Planck* and BICEP2/KECK

We use the standard cosmological Markov chain Monte Carlo (MCMC) package CosmoMC [56] along with the *Planck* 2015 likelihood [9] for our analysis. We use the *Planck* high-ℓ, Plik TTTEEE, nuisance-marginalized likelihood in the range $\ell = 30$–2508 for TT and $\ell = 30$–1996 for TE and EE, and the low-ℓTEB (TT, EE, BB and TE) likelihood in the range $\ell = 2$–29.

The BICEP2/KECK Array (BK), currently operating at 95, 150, and 220 GHz, has the tightest upper limits on the tensor-to-scalar ratio r. For our initial analysis we used BK 2015 data [11], but we were able complete our analysis using the latest BK 2018 data set [12]. In Sec. IV we elaborate on the potential tension between the BK 2015 and BK 2018 data sets in constraining the tensor parameters r and $n_{\rm t}$ (see Fig. 5). For the BK 2018 data, the *BB* band powers are split into nine multipole bins from $\ell = 37$–332 and contains a total of 12 auto and 66 cross spectra between BK 2018 maps at 95, 150, and 220 GHz, WMAP maps at 23 (K band) and 33 GHz (Ka band), and *Planck* maps at 30, 44, 70, 100, 143, 217, and 353 GHz [11,12]. We use the combined BK 2018 + *Planck* 2015 data (hereafter BKP) and the likelihood provided with CosmoMC.

We allow the six standard cosmological parameters $[\Omega_{\rm b}h^2,\ \Omega_{\rm c}h^2,\ 100\theta_*,\ \tau,\ \ln(10^{10}A_{\rm s}),\ n_{\rm s}]$ to vary in our likelihood chain. We also allow the tensor-to-scalar

[3]In Sec. 2. B. of Ref. [42] it was written that at the end of BBN, the expansion rate in the standard BBN model is 1.7 times that for photons alone, and an additional neutrino species would increase the rate by 36.7%, which we believe is incorrect.

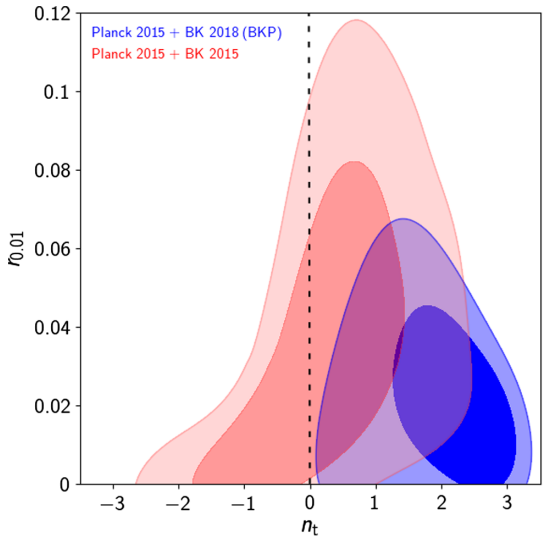

FIG. 5. The 2σ contour plot of the tensor-to-scalar ratio $r_{0.01}$ at $k = 0.01$ Mpc^{-1} and the tensor tilt n_t for the *Planck* + BICEP2 + KECK data set, where the red and blue contours represent the BICEP2/Keck 2015 and BICEP2/Keck 2018 data sets, respectively.

ratio r, the tilt of the tensor power spectrum n_t, and the effective number of relativistic species $N_{\rm eff}$ to vary in the likelihood, so essentially we have nine free parameters in total.

The default results are with only the *Planck* and BKP CMB data set mentioned above. We also combined the D/H data from Ly-α forests to tighten the constraint on $N_{\rm eff}$. We modified the CAMB/CosmoMC code to introduce the effect of additional relativistic species $\Delta N_{\rm eff}$ to the GW background as discussed in Eq. (18), and then switched this relation on and off to test the additional constraints on the tensor power spectrum. Therefore, we have four different data sets—*Planck*, *Planck*+[D/H], BKP, and BKP+[D/H]—and two models to fit: the nine-cosmological-parameter model without the $\Delta N_{\rm eff}$ relation [Eq. (18)], and the model with this relation.

IV. RESULTS OF CONSTRAINTS

We follow the *Planck* 2015 analysis on the constraints of inflation [57], relax the inflationary consistency relation, and use the $(r_{0.01}, n_t)$ parametrization, where $r_{0.01}$ is the tensor-to-scalar ratio at the decorrelation scale $k_0 = 0.01$ Mpc^{-1} for the BKP joint constraints. We summarize our joint constraints from CosmoMC runs in Figs. 5 and 6, and show the marginalized one-dimensional posterior distribution in Fig. 7. We present the quantitative values in Table I. To compare the prediction of the single-field slow-roll inflation model ($r = -8n_t$) with the current constraints, we plot this "consistency relation line" as the black dashed line in the $(r_{0.01}, n_t)$ parameter space in the left and middle panels of Figs. 5 and 6.

A. *Planck* CMB only

We first use the CMB data only from the *Planck* TT + TE + EE data sets without using the $\Delta N_{\rm eff}$ relation [Eq. (18)], and show our results using the yellow contours in the left panel of Fig. 6 and yellow lines in the upper row of Fig. 7.[4] One can see that, even without the B-mode polarization data, the *Planck* temperature and E-mode polarization data are already able to constrain $r_{0.01} < 0.60$ at 3σ C.L. This is because the primordial tensor mode can also source the temperature anisotropy before it enters the horizon, so for $\ell < \ell_{\rm R}$ [where ℓ_R is the multipole (inverse angular size) of the horizon size at recombination] there is a non-negligible contribution to the temperature anisotropy at large angular scales [58]. Therefore, the cosmic-variance-limited measurements of $C_\ell^{\rm TT}$, $C_\ell^{\rm TE}$, and $C_\ell^{\rm EE}$ place constraints on the amplitude of the primordial tensor mode.

The red contour in the left panel of Fig. 6 and the red line in the upper row of Fig. 7 use the $\Delta N_{\rm eff}$ relation [Eq. (18)] in the CosmoMC code for the *Planck*-only data case. One can see that with this relation the parameters $(r_{0.01}, n_t)$ are immediately constrained, due to the fact that the larger value of the resultant $N_{\rm eff}$ can significantly shift both the amplitude and phase of the CMB power spectrum (also see Fig. 1). As shown in Table I, $r_{0.01}$ and n_t are constrained to be $r_{0.01} < 0.155$ (3σ C.L.) and $n_t = -0.64 \pm 0.74$. This is a much tighter constraint than in the case without the $\Delta N_{\rm eff}$ relation [Eq. (18)].

B. BICEP2 + KECK Array data 2015 and 2018

The additional data from the BICEP2/KECK (BK) Array, which currently has the tightest upper limits on the B-mode power spectrum, would unequivocally improve our constraints on the above tensor parameters. As discussed in Sec. III B, we performed our MCMC runs for both the BK 2015 and 2018 data sets, and we show our results in Figs. 5 and 6. One can see from Fig. 5 that with the BK 2015 + *Planck* 2015 data set the $r_{0.01}$ parameter is constrained as $r < 0.12$ (2σ C.L.), while n_t is constrained to be center at zero but have an almost equal probability on the negative (red) and positive (blue) sides. However, with the BK 2018 + *Planck* 2015 (BKP) data set, the constraint on n_t clearly prefers a blue-tilted tensor power spectrum at $\sim 2\sigma$ C.L., as shown by the blue contours in Fig. 5 and the yellow line in the lower middle panel of Fig. 7. This has 2σ C.L. tension with the consistency relation of the single-field slow-roll inflation model.

In addition to the tilt, the r value is suppressed to $r < 0.07$ at 2σ C.L. (Table I). This is distinctly evident from the compressed two-dimensional contours for the tensor parameters when we combine the BK and *Planck* data sets,

[4]For consistency, we checked that the yellow contours in the left panel of Fig. 6 with *Planck*-only data match Fig. 59 in Ref. [57].

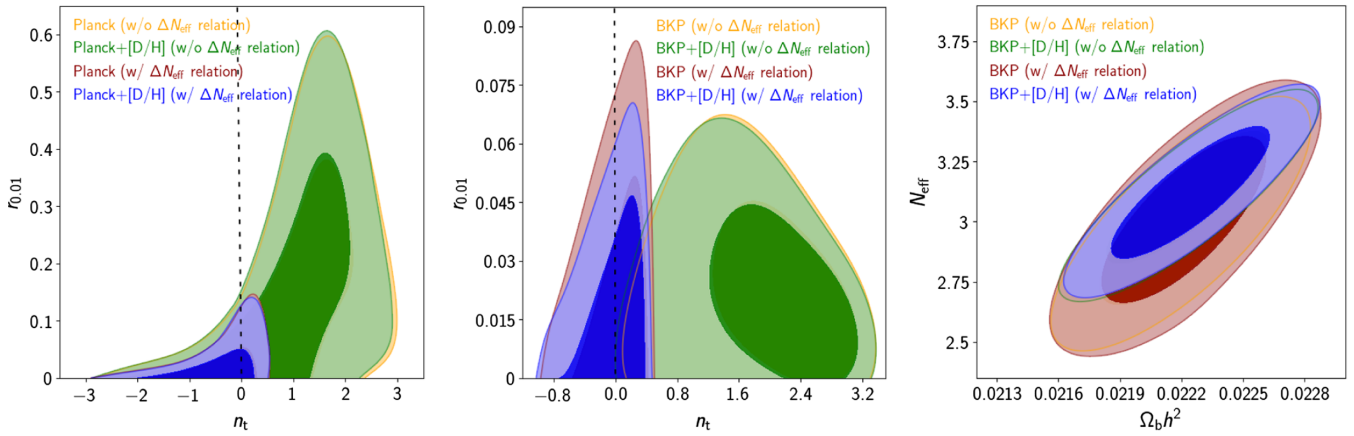

FIG. 6. 2σ contour plots for the various data sets and cases. The left and middle plots show the joint constraint of the tensor-to-scalar ratio $r_{0.01}$ and the tensor tilt n_t for the *Planck* data set and BICEP2 + KECK+*Planck* (BKP) data set, respectively. The right panel shows the joint constraint for $N_{\rm eff}$ and $\Omega_b h^2$ for the BKP data set. (The redundant results for the *Planck*-only data set are not shown.) For all plots, the four contours are for the joint constraint for the default case with CMB data only (yellow), CMB + [D/H] data (green), CMB data with the $\Delta N_{\rm eff}$ constraint (red), and CMB + [D/H] data with the $\Delta N_{\rm eff}$ constraint (blue).

as can be seen by comparing the scales of the left and middle panels of Fig. 6 (yellow contours).

But with the inclusion of the $\Delta N_{\rm eff}$ relation [Eq. (18)], the BKP constraint on $(r_{0.01}, n_t)$ is recentered at $n_t \simeq 0$ with slight favor over the red tilt, shown by the red contours in the middle panel of Fig. 6 and the red line in the middle panel of Fig. 7. r and n_t are constrained to be $r_{0.01} < 0.073$ (3σ C.L.) and $n_t = 0.01 \pm 0.31$ (1σ C.L.) for the BKP data set.

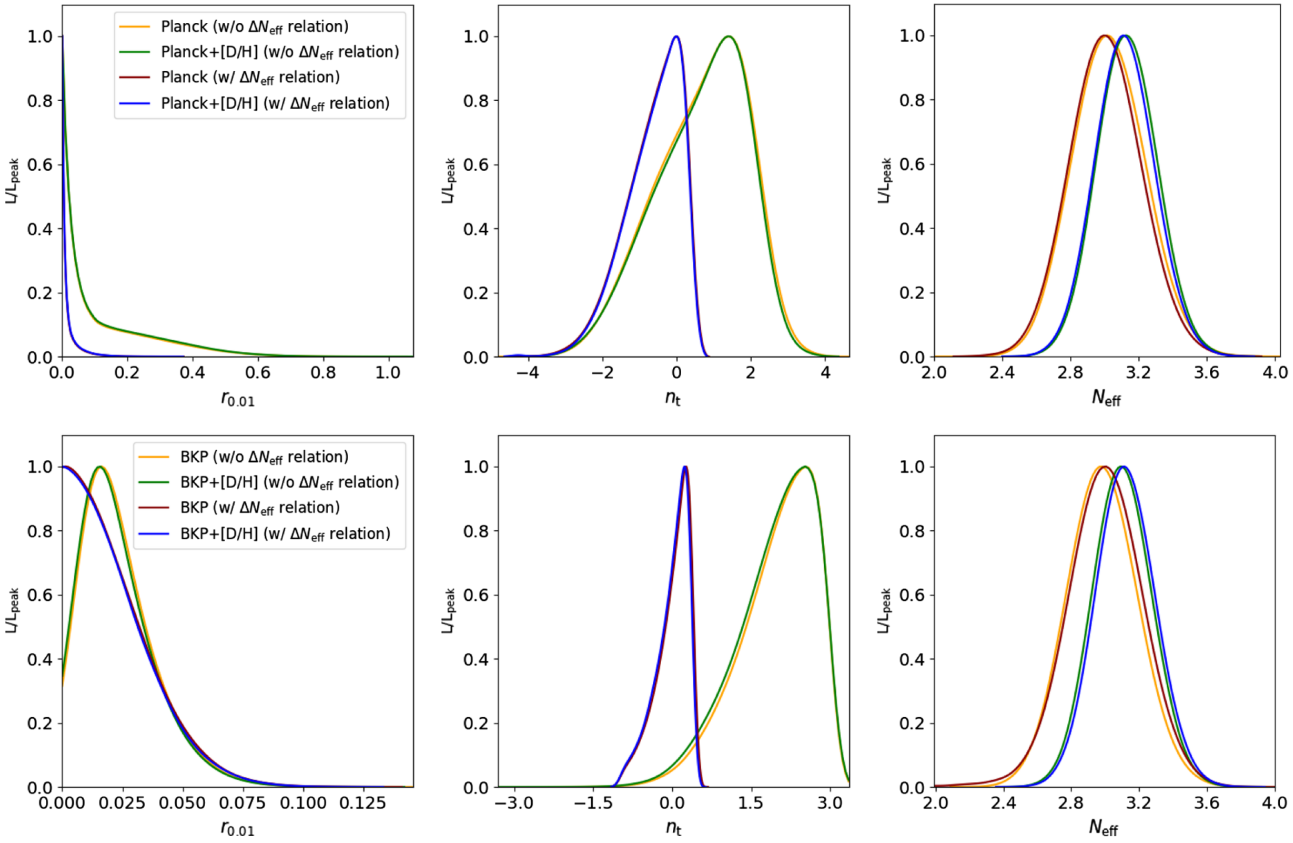

FIG. 7. The one-dimensional posterior distributions for the tensor-to-scalar ratio $r_{0.01}$, the tensor tilt n_t and the effective number of neutrino species $N_{\rm eff}$ for Top: *Planck* data set. Bottom: *Planck* + BICEP2 + KECK data set. The plots show the distributions for the default case (yellow curve), adding [D/H] data without the $\Delta N_{\rm eff}$ constraint (green curve), adding the $\Delta N_{\rm eff}$ constraint (red curve), and adding the [D/H] data with the $\Delta N_{\rm eff}$ constraint (blue curve).

TABLE I. Marginalized values of cosmological parameters, effective neutrinos, and $\log \mathcal{L}$ values using various combinations of *Planck*, *Planck* + BICEP2 + KECK (BKP), and deuterium data sets, with and without the $\Delta N_{\rm eff}$ equation. The value quoted for $r_{0.01}$ is the 3σ upper limit value for the tensor-to-scalar ratio at the pivot scale $k_0 = 0.01$ Mpc^{-1}.

Parameters	$\Delta N_{\rm eff}$ relation	*Planck*	*Planck* + [D/H]	BKP	BKP + [D/H]
$\Omega_{\rm b}h^2$	No	0.0222 ± 0.0002	0.0223 ± 0.0002	0.0222 ± 0.0002	0.0222 ± 0.0002
	Yes	0.0222 ± 0.0002	0.0222 ± 0.0002	0.0222 ± 0.0002	0.0222 ± 0.0002
$A_{\rm s}$	No	3.09 ± 0.04	3.10 ± 0.04	3.09 ± 0.04	3.10 ± 0.04
	Yes	3.09 ± 0.04	3.09 ± 0.04	3.10 ± 0.04	3.10 ± 0.04
$r_{0.01}$	No	<0.598	<0.492	<0.070	<0.069
	Yes	<0.155	<0.156	<0.073	<0.073
$n_{\rm t}$	No	0.68 ± 1.22	0.66 ± 1.20	2.00 ± 0.72	1.97 ± 0.74
	Yes	-0.64 ± 0.74	-0.64 ± 0.74	0.01 ± 0.31	-0.01 ± 0.31
$N_{\rm eff}$	No	3.026 ± 0.209	3.132 ± 0.172	2.985 ± 0.204	3.103 ± 0.171
	Yes	3.005 ± 0.207	3.118 ± 0.172	3.000 ± 0.219	3.122 ± 0.171
$-\log \mathcal{L}$	No	5527	5528	5895	5896
	Yes	5529	5529	5897	5897

C. Deuterium abundance data

We further include the deuterium abundance measurement [44] [Eq. (22)] to tighten up the constraints. The deuterium abundance is sensitive to the baryon density $\Omega_{\rm b}h^2$ and $N_{\rm eff}$, which can affect the constraints on r and $n_{\rm t}$ since these parameters are correlated. We first include the [D/H] measurement for the *Planck*-only data case in the left panel of Fig. 6 and upper row of Fig. 7. The addition of [D/H] data does not improve the constraints too much.

However, the effect of [D/H] data kicks in when we use the BKP data sets with the inclusion of the $\Delta N_{\rm eff}$ relation [Eq. (18)], as shown in the middle panel of Fig. 6 and lower row of Fig. 7. Comparing the red and blue contours in the middle panel of Fig. 6, the upper limit of r is further constrained with the additional [D/H] data set. The tightest constraints on r and $n_{\rm t}$ become $r_{0.01} < 0.073$ (3σ C.L.) and $n_{\rm t} = -0.01 \pm 0.31$ (1σ C.L.), respectively. We also plot the inflation consistency relation in the middle panel of Fig. 6 (black dashed line). One can see that the current BKP + [D/H] data with the $\Delta N_{\rm eff}$ relation contains this line as its center, indicating that the current data is still consistent with the single-field slow-roll inflation scenario but does not exclude other scenarios.

Besides the $(r, n_{\rm t})$ constraints, the addition of the [D/H] data set can also tighten up the $N_{\rm eff} - \Omega_{\rm b}h^2$ joint constraints, as seen in the right panel of Fig. 6. [D/H] data provide much tighter constraints on $N_{\rm eff}$ than the CMB data alone. From Table I we see that the positive value of $\Delta N_{\rm eff}$ from the CosmoMC runs falls well within the theoretical values, as seen in Fig. 4. The tightest constraint on $N_{\rm eff}$ is $N_{\rm eff} = 3.122 \pm 0.177$ for the current BKP + [D/H] data with the $\Delta N_{\rm eff}$ relation, excluding the fourth species of neutrino/relativistic particle at more than 5σ C.L.

The other cosmological parameters (such as $\Omega_{\rm c}h^2$, $100\theta_{\rm MC}$, $A_{\rm s}$, $n_{\rm s}$, and τ) are not strongly affected by including the $\Delta N_{\rm eff}$ relation, so we do not present the results for these parameters here, though we vary them in the likelihood chain. We refer the interested reader to Refs. [9,11,12], which arrived at equivalent constraints.

V. DISCUSSION AND CONCLUSIONS

In this work we proposed a new relation between the amplitude (r) and tilt ($n_{\rm t}$) of the primordial tensor power spectrum with the additional effective number of relativistic degrees of freedom ($\Delta N_{\rm eff}$). The reason is that a bluer tilt leads to an increase in the degrees of freedom of the stochastic primordial GW background, which will act like additional neutrino species, boosting the value of $N_{\rm eff}$ ($N_{\rm eff} = N_\nu + \Delta N_{\rm eff}$, where $N_\nu = 3.046$). This results in an increased production of primordial deuterium and enhances the CMB damping tail in the temperature power spectrum. Combined with the CMB polarization power spectrum, one can place tight and reliable constraints on r and $n_{\rm t}$.

We point out that our constraints on the initial GW parameters depend on the prior we used on r, as the tensor perturbation power spectrum has not been detected. We used a flat prior on r, varying it from 0 to 2 for the *Planck*-only case, and from 0 to 0.5 for the BKP case. Indeed, this cannot explore the parameter space where r is less than some threshold, and therefore the posterior distribution function of $n_{\rm t}$ goes to zero. However, the constraints are reliable even if the lower bound of r is 10^{-3}–10^{-4}, e.g., $r \sim 10^{-3}$ for Starobinsky inflation [59], as our MCMC chains have adequate samples to explore that range.

In this work we used the *Planck* 2015 likelihood chain, combined with BICEP2/KECK Array 2018 data and [D/H] measurements from DLA systems to place constraints on r, $n_{\rm t}$, and $N_{\rm eff}$. We first showed the results for *Planck*-only constraints, and then added the BK results of 2015 and 2018, and finally added the [D/H] measurements for both the cases with and without the $\Delta N_{\rm eff}$ relation [Eq. (18)]. One can see that, even without the BK result, the inclusion of the $\Delta N_{\rm eff}$ relation [Eq. (18)] significantly improves the constraints on $(r, n_{\rm t})$. With the additional BK data, the constraints on $r_{0.01}$

and n_t are further tightened up. With the additional [D/H] data, the tightest constraints are $r < 0.073$ (3σ C.L.) and $n_t = -0.01 \pm 0.31$ (1σ C.L.). This already places stringent constraints on inflation models, as it still favors the single-field slow-roll inflation model. The tightest constraint on $N_{\rm eff}$ is $N_{\rm eff} = 3.122 \pm 0.171$ for BKP2018 + [D/H] data, excluding the fourth species of neutrino at high significance.

We compared our results with the upper limits on $\Omega_{\rm gw}h^2 < 1.2 \times 10^{-6}$ at the 95% confidence limit (as discussed in Ref. [60]), where $\Omega_{\rm gw}$ is used as the total tensor mode across all frequencies. In Eq. (4) we defined $\Omega_{\rm gw}$ as a function of k. Using Eqs. (4) and (8), the total tensor mode across all frequencies is given as $\Omega_{\rm gw}h^2 = \int d\ln k \Omega_{\rm gw}(k)h^2 = \Delta N_{\rm eff}h^2/(1.781 \times 10^5)$. Since we finally obtained $\Delta N_{\rm eff} < 0.418$ (BKP + D/H; Table I), we have $\Omega_{\rm gw}h^2 < (2.3 \times 10^{-6})h^2$ at the 95% confidence limit. With $h = 0.68$, we have $\Omega_{\rm gw}h^2 < 1.06 \times 10^{-6}$, which is consistent (slightly tighter) with the result from Ref. [60].

The combination of direct and indirect measurements from future experiments will put stronger constraints on stochastic GWs at different frequencies. Future CMB experiments (such as the Simons Observatory [61] and COrE [62]) will improve the measurements of the polarization of the CMB and further constrain the limits on r and n_t. With the $\Delta N_{\rm eff}$ relation proposed in this work, measurements of the primordial helium and deuterium abundances will provide stringent constraints on the tensor parameters, indirectly shedding light on the stochastic GW background. In the higher-frequency part of the spectrum, direct measurements from GW experiments over a large range of frequencies [63] (including the ground-based LIGO [19] and space-based interferometers like the Laser Interferometer Space Antenna [64]) will also put constraints on the stochastic GW background. The combination of these experiments will result in stringent tests of gravitational radiation and early Universe physics.

ACKNOWLEDGMENTS

We thank the anonymous referee for useful suggestions to the article. We thank Kris Sigurdson for suggestions at an early stage of this work, Ryan Cooke for discussion on deuterium measurement and primordial abundance, and Antony Lewis, Fabio Finelli and Jussi Valiviita for discussions on the *Planck* 2015 likelihood and CosmoMC. We thank Antony Lewis for the use of the publicly available numerical codes CosmoMC and CAMB. We acknowledge the use of *hippo*, UKZN's high-performance computing facility. M.A. acknowledges the Claude Leon Foundation, South Africa, and the South African Radio Astronomy Observatory (SARAO), under National Research Foundation (NRF) Grant No. 95393 under Kavilan Moodley at UKZN. Y. Z. M. acknowledges support by the NRF from Grants No. 105925 and 120378, and the National Science Foundation of China under Grant No. 11828301.

[1] E. J. Copeland, E. W. Kolb, A. R. Liddle, and J. E. Lidsey, Phys. Rev. Lett. **71**, 219 (1993).
[2] R. H. Brandenberger, A. Nayeri, S. P. Patil, and C. Vafa, Phys. Rev. Lett. **98**, 231302 (2007).
[3] M. Baldi, F. Finelli, and S. Matarrese, Phys. Rev. D **72**, 083504 (2005).
[4] A. Stewart and R. Brandenberger, J. Cosmol. Astropart. Phys. 08 (2008) 012.
[5] L. A. Boyle, P. J. Steinhardt, and N. Turok, Phys. Rev. D **69**, 127302 (2004).
[6] J.-L. Lehners, Phys. Rep. **465**, 223 (2008).
[7] S. Kuroyanagi, T. Takahashi, and S. Yokoyama, J. Cosmol. Astropart. Phys. 02 (2015) 003.
[8] P. A. R. Ade, N. Aghanim, M. Arnaud, M. Ashdown, J. Aumont, C. Baccigalupi, A. J. Banday, R. B. Barreiro, J. G. Bartlett *et al.* (Planck Collaboration), Astron. Astrophys. **594**, A13 (2016).
[9] N. Aghanim, M. Arnaud, M. Ashdown, J. Aumont, C. Baccigalupi, A. J. Banday, R. B. Barreiro, J. G. Bartlett, N Bartolo *et al.* (Planck Collaboration), Astron. Astrophys. **594**, A11 (2016).
[10] N. Aghanim, Y. Akrami, M. Ashdown, J. Aumont, C. Baccigalupi, M. Ballardini, A. J. Banday, R. B. Barreiro, N. Bartolo *et al.* (Planck Collaboration), arXiv: 1807.06209.
[11] P. A. R. Ade, N. Aghanim, Z. Ahmed, R. W. Aikin, K. D. Alexander, M. Arnaud, J. Aumont, C. Baccigalupi *et al.* (BICEP2/Keck and Planck Collaborations), Phys. Rev. Lett. **114**, 101301 (2015).
[12] P. A. R. Ade, Z. Ahmed, R. W. Aikin, K. D. Alexander, D. Barkats, S. J. Benton, C. A. Bischoff, J. J. Bock, R. Bowens-Rubin, J. A. Brevik *et al.* (Keck Array and Bicep2 Collaborations), Phys. Rev. Lett. **121**, 221301 (2018).
[13] B. Allen, in *Relativistic Gravitation and Gravitational Radiation*, edited by J.-A. Marck and J.-P. Lasota (1997), p. 373, https://arxiv.org/abs/gr-qc/9604033.
[14] M. Maggiore, Phys. Rep. **331**, 283 (2000).
[15] P. B. Demorest, R. D. Ferdman, M. E. Gonzalez, D. Nice, S. Ransom, I. H. Stairs, Z. Arzoumanian, A. Brazier, S. Burke-Spolaor, S. J. Chamberlin *et al.*, Astrophys. J. **762**, 94 (2013).
[16] W. Zhao, Y. Zhang, X.-P. You, and Z.-H. Zhu, Phys. Rev. D **87**, 124012 (2013).

[17] P. D. Meerburg, R. Hložek, B. Hadzhiyska, and J. Meyers, Phys. Rev. D **91**, 103505 (2015).
[18] L. A. Boyle and A. Buonanno, Phys. Rev. D **78**, 043531 (2008).
[19] B. P. Abbott, R. Abbott, T. D. Abbott, M. R. Abernathy, F. Acernese, K. Ackley, C. Adams, T. Adams, P. Addesso, R. X. Adhikari *et al.*, Phys. Rev. Lett. **118**, 121101 (2017).
[20] M. Giovannini, Classical Quantum Gravity **16**, 2905 (1999).
[21] K. N. Abazajian, K. Arnold, J. Austermann, B. A. Benson, C. Bischoff, J. Bock, J. R. Bond, J. Borrill, E. Calabrese, J. E. Carlstrom *et al.*, Astropart. Phys. **63**, 66 (2015).
[22] M. Costanzi, B. Sartoris, M. Viel, and S. Borgani, J. Cosmol. Astropart. Phys. 10 (2014) 081.
[23] V. Simha and G. Steigman, J. Cosmol. Astropart. Phys. 06 (2008) 016.
[24] S. Dodelson, *Modern Cosmology* (Academic Press, Amsterdam, 2003).
[25] E. Komatsu, J. Dunkley, M. R. Nolta, C. L. Bennett, B. Gold, G. Hinshaw, N. Jarosik, D. Larson, M. Limon, L. Page *et al.*, Astrophys. J. Suppl. Ser. **180**, 330 (2009).
[26] B. Follin, L. Knox, M. Millea, and Z. Pan, Phys. Rev. Lett. **115**, 091301 (2015).
[27] D. Baumann, D. Green, and M. Zaldarriaga, J. Cosmol. Astropart. Phys. 11 (2017) 007.
[28] D. Baumann, D. Green, and B. Wallisch, J. Cosmol. Astropart. Phys. 08 (2018) 029.
[29] S. Henrot-Versillé, F. Couchot, X. Garrido, H. Imada, T. Louis, M. Tristram, and S. Vanneste, Astron. Astrophys. **623**, A9 (2019).
[30] C. D. Kreisch, F.-Y. Cyr-Racine, and O. Doré, https://arxiv.org/abs/1902.00534.
[31] G. Hinshaw, D. Larson, E. Komatsu, D. N. Spergel, C. L. Bennett, J. Dunkley, M. R. Nolta, M. Halpern, R. S. Hill, N. Odegard *et al.*, Astrophys. J. Suppl. Ser. **208**, 19 (2013).
[32] Y. Akrami, F. Arroja, M. Ashdown, J. Aumont, C. Baccigalupi, M. Ballardini, A. J. Banday, R. B. Barreiro, N. Bartolo *et al.* (Planck Collaboration), *Planck 2018 Results. I. Overview and the Cosmological Legacy of Planck* (2018), https://doi.org/10.1051/0004-6361/201833880.
[33] E. Calabrese, R. A. Hložek, J. R. Bond, M. J. Devlin, J. Dunkley, M. Halpern, A. D. Hincks, K. D. Irwin, A. Kosowsky, K. Moodley *et al.*, Phys. Rev. D **95**, 063525 (2017).
[34] T. Louis, E. Grace, M. Hasselfield, M. Lungu, L. Maurin, G. E. Addison, P. A. R. Ade, S. Aiola, R. Allison, M. Amiri *et al.*, J. Cosmol. Astropart. Phys. 06 (2017) 031.
[35] F. Bianchini, W. L. K. Wu, P. A. R. Ade, A. J. Anderson, J. E. Austermann, J. S. Avva, J. A. Beall, A. N. Bender, B. A. Benson, L. E. Bleem *et al.*, Astrophys. J. **888**, 119 (2019).
[36] G. Simard, Y. Omori, K. Aylor, E. J. Baxter, B. A. Benson, L. E. Bleem, J. E. Carlstrom, C. L. Chang, H.-M. Cho, R. Chown *et al.*, Astrophys. J. **860**, 137 (2018).
[37] B. P. Crill, P. A. R. Ade, E. S. Battistelli, S. Benton, R. Bihary, J. J. Bock, J. R. Bond, J. Brevik, S. Bryan, C. R. Contaldi *et al.*, Space Telescopes and Instrumentation 2008: Optical, Infrared, and Millimeter (2008), https://doi.org/10.1117/12.787446.
[38] J. P. Filippini, P. A. R. Ade, M. Amiri, S. J. Benton, R. Bihary, J. J. Bock, J. R. Bond, J. A. Bonetti, S. A. Bryan, B. Burger *et al.*, Millimeter, Submillimeter, and Far-Infrared Detectors and Instrumentation for Astronomy V (2010), https://doi.org/10.1117/12.857720.
[39] R. Gualtieri, J. P. Filippini, P. A. R. Ade, M. Amiri, S. J. Benton, A. S. Bergman, R. Bihary, J. J. Bock, J. R. Bond, S. A. Bryan *et al.*, J. Low Temp. Phys. **193**, 1112 (2018).
[40] R. Keisler, C. L. Reichardt, K. A. Aird, B. A. Benson, L. E. Bleem, J. E. Carlstrom, C. L. Chang, H. M. Cho, T. M. Crawford, A. T. Crites *et al.*, Astrophys. J. **743**, 28 (2011).
[41] Z. Hou, R. Keisler, L. Knox, M. Millea, and C. Reichardt, Phys. Rev. D **87**, 083008 (2013).
[42] K. M. Nollett and G. P. Holder, arXiv:1112.2683.
[43] R. J. Cooke, M. Pettini, K. M. Nollett, and R. Jorgenson, Astrophys. J. **830**, 148 (2016).
[44] R. J. Cooke, M. Pettini, and C. C. Steidel, Astrophys. J. **855**, 102 (2018).
[45] T. L. Smith, M. Kamionkowski, and A. Cooray, Phys. Rev. D **73**, 023504 (2006).
[46] E. W. Kolb and M. S. Turner, Front. Phys. **69**, 1 (1990).
[47] Y.-Z. Ma, W. Zhao, and M. L. Brown, J. Cosmol. Astropart. Phys. 10 (2010) 007.
[48] R. V. Wagoner, W. A. Fowler, and F. Hoyle, Astrophys. J. **148**, 3 (1967).
[49] E. Aver, K. A. Olive, and E. D. Skillman, J. Cosmol. Astropart. Phys. 07 (2015) 011.
[50] E. Aver, K. A. Olive, R. L. Porter, and E. D. Skillman, J. Cosmol. Astropart. Phys. 11 (2013) 017.
[51] R. J. Cooke, M. Pettini, R. A. Jorgenson, M. T. Murphy, and C. C. Steidel, Astrophys. J. **781**, 31 (2014).
[52] L. Sbordone, P. Bonifacio, E. Caffau, H. G. Ludwig, N. T. Behara, J. I. González Hernández, M. Steffen, R. Cayrel, B. Freytag, C. van't Veer *et al.*, Astron. Astrophys. **522**, A26 (2010).
[53] K. A. Olive and E. D. Skillman, Astrophys. J. **617**, 29 (2004).
[54] L. E. Marcucci, G. Mangano, A. Kievsky, and M. Viviani, Phys. Rev. Lett. **116**, 102501 (2016).
[55] O. Pisanti, A. Cirillo, S. Esposito, F. Iocco, G. Mangano, G. Miele, and P. Serpico, Comput. Phys. Commun. **178**, 956 (2008).
[56] A. Lewis and S. Bridle, Phys. Rev. D **66**, 103511 (2002).
[57] P. A. R. Ade, N. Aghanim, M. Arnaud, F. Arroja, M. Ashdown, J. Aumont, C. Baccigalupi, M. Ballardini, A. J. Banday *et al.* (Planck Collaboration), Astron. Astron. **594**, A20 (2016).
[58] J. R. Pritchard and M. Kamionkowski, Ann. Phys. (Amsterdam) **318**, 2 (2005).
[59] A. A. Starobinsky, Sov. Astron. Lett. **9**, 302 (1983), https://inspirehep.net/record/199078/.
[60] L. Pagano, L. Salvati, and A. Melchiorri, Phys. Lett. B **760**, 823 (2016).
[61] P. Ade, J. Aguirre, Z. Ahmed, S. Aiola, A. Ali, D. Alonso, M. A. Alvarez, K. Arnold, P. Ashton, J. Austermann *et al.*, J. Cosmol. Astropart. Phys. 02 (2019) 056.
[62] C. Armitage-Caplan, M. Avillez, D. Barbosa, A. Banday, N. Bartolo, R. Battye, J. Bernard, P. de Bernardis, S. Basak *et al.*, Core (Cosmic Origins Explorer) A White Paper (2011), https://arxiv.org/abs/1102.2181.
[63] G. Cabass, L. Pagano, L. Salvati, M. Gerbino, E. Giusarma, and A. Melchiorri, Phys. Rev. D **93**, 063508 (2016).
[64] N. Bartolo, C. Caprini, V. Domcke, D. G. Figueroa, J. Garcia-Bellido, M. C. Guzzetti, M. Liguori, S. Matarrese, M. Peloso, A. Petiteau *et al.*, J. Cosmol. Astropart. Phys. 12 (2016) 026.